Cancer Nanotechnology

RESEARCH Open Access

Green synthesis of oncolytic Newcastle disease virus-loaded thiolated chitosan nanoformulation for CD44 targeted delivery and sustained release of virus in cervical cancer xenografts

Kousain Kousar[1*], Faiza Naseer[1,2], Maisa S. Abduh[3,4], Sadia Anjum[5] and Tahir Ahmad[1*]

*Correspondence:
kousain777@outlook.com;
tahir@asab.nust.edu.pk;
baig42@gmail.com

[1] Industrial Biotechnology, Atta-Ur-Rahman School of Applied Biosciences, National University of Sciences and Technology, Islamabad, Pakistan
[2] Shifa College of Pharmaceutical Sciences, Shifa Tameer-E-Millat University, Islamabad, Pakistan
[3] Immune Responses in Different Diseases Research Group, Department of Medical Laboratory Sciences, Faculty of Applied Medical Sciences, King Abdul-Aziz University, Jeddah 21589, Saudi Arabia
[4] Center of Excellence in Genomic Medicine Research, King Abdulaziz University, Jeddah, Saudi Arabia
[5] Department of Biology, University of Hail, Hail, Saudi Arabia

Abstract

Background: Newcastle disease virus (NDV) Lasota strain has proven oncolytic activity. One shortcoming associated with this treatment modality is the immune neutralization of the virus in body, mediated by natural killer cells and macrophages. This study aims at encapsulating the oncolytic virus in thiolated chitosan nanoparticles, surface functionalized with hyaluronic acid for CD44 targeted delivery and sustained release of NDV in cervical cancer tumors. These nanoparticles were tested for oncolytic potential in HeLa cells and cervical cancer xenograft model.

Results: NDV-loaded nanoparticles were prepared using TCs concentration of 1.0 mg/mL, HA at 0.5 mg/mL, with a half dose (not less than 500 TCID units) of NDV by using green synthesis approach through ionic gelation method. Viral quantification in nanoparticles was done by $TCID_{50}$ (50% tissue culture infectious dose) and MOI (multiplicity of infection) determination. Ex vivo NK cell activity was analyzed by quantifying levels of IFN-γ. In vivo analysis was performed on wistar rats, immunocompromised by using ketoconazole (10 mg/kg) and cyclosporin (30 mg/kg) along with 0.1 µg/mL of amoxicillin. WBC profiling on day 7 confirmed immunosuppression, which was followed by tumor implantation. Zeta analysis of NDV nanoparticles showed that nanoparticles are 286.9 nm in size with a zeta potential of 18.1 mV and PDI of 0.241. For estimation of anticancer potential, MTT and trypan blue exclusion assay revealed a higher cytotoxic potential of the encapsulated virus, while $TCID_{50}$ of HA-TC-NDV was 4.1 as compared to naked NDV virus which had $TCID_{50}$ of 6.0 on HeLa cells. Histopathology of organs from NDV nanoparticle-treated rats showed syncytia formation in tumors, immunohistochemical analysis showed decrease in expression of TNF-α, COX-II and NF-ℜB which was also confirmed by ELISA. RT-PCR showed high viral copy number in tumor tissue and viral accumulation in lungs and liver. Lower IFN-γ in nanoparticles treated rats showed suppression in immunoreactivity of virus-loaded nanoparticles.

Conclusion: Our findings suggest that encapsulation of the virus in thiolated chitosan and CD44 targeting enhanced retention and sustained release of the virus in tumors as compared to pure NDV, with increased oncolytic effect both in vitro and in vivo.

Keywords: Oncolytic NDV, Virus encapsulation, Thiolated chitosan, Immune neutralization, CD44

Background

According to global cancer observatory data, carcinoma of cervix is the 5th major cause of death in women of reproductive age. As per the Human Papilloma Virus (HPV) Information Centre, approximately 199,902 cases of cervical cancer are annually diagnosed in Asia. In spite of preventive vaccination programs and advanced treatment options, it is still the fourth major cause of death in Asian women and the third leading gynecological cancer in women aged 15–45 (Global Cancer Observatory 2020) (Human Papillomavirus and Related Diseases Report ASIA 2019). Although the current treatment regimen has substantially controlled the disease progression and associated mortality rate, the need for better treatment modalities for targeted anticancer therapies with fewer adverse effect still remains. Immunotherapy is currently the most focused approach in cancer treatment regimens, which utilizes various methodologies to reprogram the immune system and its components against cancer cells (Schmidt et al. 2022). Oncolytic viruses have gained attention as immunotherapy agents owing to their ability to target cancer cells selectively, infect neighboring cells after tumor cell lysis and stimulate both innate and adaptive immunity towards the tumor microenvironment (TME) (Keshavarz et al. 2020).

Newcastle disease virus (NDV) is nonpathogenic in mammals and has demonstrated promising oncolytic potential in solid malignancies such as prostate, breast, ovarian, and cervical cancer, ranking them suitable for anticancer virotherapy (Chan et al. 2021). There are three different pathotypes of the NDV virus: velogenic, mesogenic and lentogenic. Velogenic strain is naturally attenuated, mesogenic is mildly pathogenic, while lentogenic is highly pathogenic in birds. Oncolytic NDV destroys tumor microenvironment by inducing local inflammation at the tumor site, releasing DAMPs (damage-associated molecular patterns), PAMPs (pathogen-associated molecular patterns), and cytokines which stimulate both innate and adaptive immune system (Vijayakumar and Zamarin 2019) (Liu et al. 2020). A major setback associated with oncolytic virotherapy is the neutralization of the virus by the host immune system. This problem can be solved by encapsulating the virus in a nano-drug delivery system. A nano-drug delivery system can be customized for sustained virus release in TME and targeted delivery only to the tumor cells (Shin et al. 2021).

Biodegradable, biocompatible polymer such as chitosan have been explored as drug delivery systems owing to their mucoadhesive nature and property of sustained release. Encapsulation of the oncolytic viruses in polymeric drug delivery systems is a promising approach as it masks viruses from immune reaction (Naseer et al. 2023). These polymeric NPs can be targeted against specific receptors that are overexpressed on cancer cells by surface functionalization with different moieties, such as folic acid for folate receptor targeting and hyaluronic acid for CD44 targeting. Such a nano-delivery system offers various advantages that include (i) increased circulation time; (ii) reduced off-target effects; (iii) sustained

release and slow clearance of the virus from tumor microenvironment; (iv) active targeting of cancer cells resulting in an increased oncolytic effect (Kousar et al. 2023).

Genetically modified animal models or immune-deficient nude mice have been used to develop cancer xenograft models to test different treatment modalities. It has been reported that nude mice might not be very suitable as tumor xenograft models as they lack some major immune players that play a critical role in tumorigenesis. Other drawbacks include a high mortality rate, limited availability and maintenance of a sterile environment, high graft rejection tendency and scarcity of resources for genetic modification in underdeveloped countries (Sayyed et al. 2021). However, immunosuppression in animal models can also be achieved through neonatal thymectomy, immunosuppressive drugs (procarbazine, cyclosporin, cyclophosphamide, etc.) and radiation. Therefore, in our current research, we prepared a tumor xenograft model by inducing pharmacological immunosuppression using ketoconazole and cyclosporine, following a previously published protocol for preparing a tumor xenograft model (Aghasizadeh et al. 2022).

The immunosuppressive drug cyclosporine acts by inhibiting the release of interleukin 1 and 2 from macrophages, which is required for the activation and proliferation of T lymphocytes (Liddicoat and Lavelle 2019). Another potent immunosuppressant, cyclophosphamide, selectively suppresses antigen-specific killer T lymphocytes (Yan et al. 2021). For the current study, a reproducible and versatile immunosuppression protocol was adopted to produce a cervical cancer xenograft model in mice. The immunosuppression was achieved by co-administration of cyclosporin, cyclophosphamide and ketoconazole (an antifungal drug).

HeLa cells, a cervical cancerous cell line isolated from a patient in 1951, is the most commonly used cellular model for cervical cancer. They are also used to analyze the anticancer potential of various therapeutic modalities and to develop the cervical cancer xenograft model (Cilwyn-Shalitha and Sasidharan 2023). Like many other solid malignancies, HeLa cells also exhibit a high expression of CD44 and thus can be used to evaluate CD44 targeted efficacy of our nanoformulation (Yoon et al. 2022).

This study evaluated the antitumor potential of the NDV-loaded thiolated chitosan NPs coated with hyaluronic acid (HA-TCs-NDV) in HeLa cells and in cervical cancer xenograft rat model. For this purpose, nanoparticles were synthesized using green synthesis protocol as polymers from natural sources were used for synthesis of nanoparticles and no harsh chemicals, acids/alkalis were used or produced during synthesis process. The analysis included in vitro evaluation of anticancer potential in HeLa cells, estimation of ex vivo immunoreactivity and, in vivo target binding and oncolytic potential of HA-TCs-NDV in pharmacologically immunosuppressed xenograft model. Owing to the targeting capacity, the ability to mask the virus from immune neutralization, and the sustained release of virus for a longer duration, this nano-delivery system may prove to be a stepping stone for enhancing the therapeutic outcomes of oncolytic virotherapy in cancer treatment regimen.

Results

Physiochemical characterization

The **s**ize, shape and polydispersity index (PDI) of TC-NDV and HA-TC-NDV were characterized using a zeta sizer. The average particle size of TC-NDV was 270.9 nm, with 19.2 mV zeta potential and 0.21 PDI as shown in Fig. 1A, C. While the average particle

size for HA-TC-NDV was found to be 286.9 nm with a zeta potential of 18.1 mV and PDI of 0.241 as shown Fig. 1B, D, at TCs concentration of 1.0 mg/mL, HA at 0.5 mg/mL, with a half dose (not less than 500 TCID units) of NDV.

Multiplicity of infection (MOI) and $TCID_{50}$

HeLa cells were infected with pure NDV and HA-TC-NDV at various MOIs (0.6, 1, 5, 8, 12,18, 20), and the resulting growth inhibition was calculated. A shown in Fig. 2A, the growth inhibition due to HA-TC-NDV was greater than pure NDV as the MOI increased.

$TCID_{50}$ of HA-TC-NDV in comparison with pure NDV was determined by infecting cells at different concentrations, cytotoxic effect in infected HeLA cells was investigated at 7 p.d.i by Reed and Muench protocol. The reported $TCID_{50}$ of pure NDV and HA-TC-NDV was 6.0 and 4.1, respectively, on HeLa cells as shown in Fig. 2B.

Trypan Blue exclusion assay

The targeted anticancer potential of NDV nanoformulation was analyzed by testing pure NDV and HA-TC-NDV on HeLa cells. The lowest cell viability of $15 \pm 0.06\%$ was observed at 85 µg/mL concentration when treated with HA-TC-NDV, while the cell viability at same concentration (MOI) of pure NDV was 24 ± 0.81. The highest cell viability of $83 \pm 0.12\%$ was observed at 15 µg/mL of HA-TC-NDV, while the cells treated with pure NDV at same concentration (MOI) exhibited cell viability of $90 \pm 0.27\%$. The oncolytic effect of nanoformulation encapsulated virus was greater than that of pure NDV on HeLa cells, as shown in Table 1

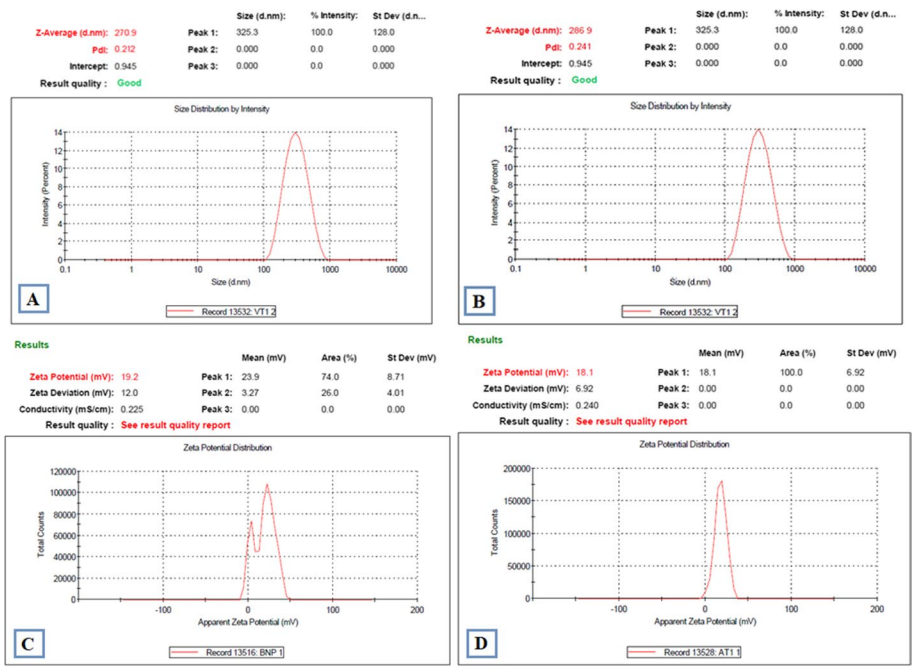

Fig. 1 Zeta analysis. **A** Particle size and PDI of TC-NDV NPs; **B** particle size and PDI of HA-TC-NDV nanoparticles; **C** zeta potential of TC-NDV NPs; **D** zeta potential of HA-TC-NDV NPs ($n = 5$, mean + SD, $p \leq 0.05$)

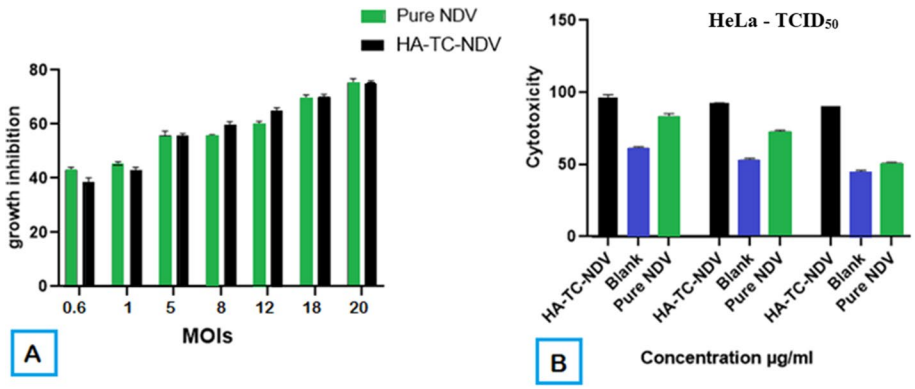

Fig. 2 **A** Growth inhibition in HeLa cells due to HA-TC-NDV and pure NDV at different MOIs. **B** Calculation of $TCID_{50}$ for HA-TC-NDV and pure NDV in HeLa cells ($n = 3$, mean + SD, $p \leq 0.05$)

Table 1 Cell viability analysis of pure NDV and HA-TC-NDV at different concentrations ($n = 3$, mean + SD, $p \leq 0.05$)

S. no.	Concentration (µg/mL)	HA-TC-NDV	Pure NDV
% cell viability			
1	85	15 ± 0.06	24 ± 0.81
2	50	42 ± 0.38	49 ± 0.49
3	15	83 ± 0.12	90 ± 0.27
4	0	93 ± 0.07	93 ± 0.07

MTT cytotoxicity assay

Cells were treated with different concentrations (15, 30, 50, 70, and 85 µg/mL) of HA-TC-NDV and pure NDV to evaluate cytotoxicity. It was noted that the cytotoxicity of cells increased in a dose-dependent manner. The highest cytotoxicity was observed at 85 µg/mL concentration, while the lowest was recorded at 15 µg/mL. The oncolytic effect of nanoformulation-loaded NDV on HeLa cells was more significant as compared to pure NDV as shown (Fig. 3).

Immunosuppression confirmation by WBC profiling

The co-administration of ketoconazole (10 mg/kg) and cyclophosphamide (30 mg/kg) induced significant immunosuppression in animals in a dose-dependent manner. Immunosuppression did not result in any signs of cytotoxicity or mortality. As per the blood analysis from healthy animals, mean WBC, lymphocyte, and neutrophil count was 7.37 ± 0.02, 6.67 ± 0.03 and $4.21 \pm 0.01 \times 10^3$ cells/µL, respectively, as shown in Fig. 4. The mentioned counts were reduced after 18 h, while on day 7, the counts had reduced to 1.51 ± 0.01, 0.79 ± 0.01 and $0.95 \pm 0.02 \times 10^3$ cells/µL for mean WBC, lymphocyte and neutrophils count, respectively. At the end of the protocol, complete immunosuppression was achieved by administration of cyclophosphamide on days 1 and 3 at 60 mg/kg dose before tumor implantation, as depicted in Fig. 4.

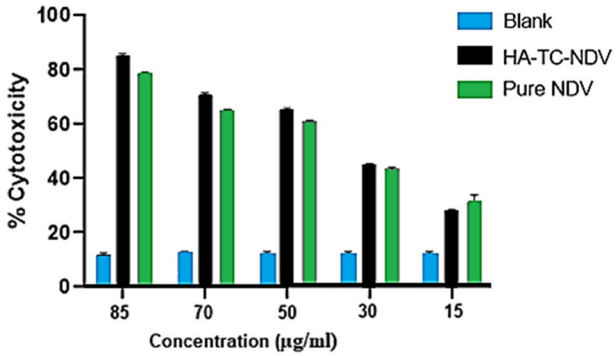

Fig. 3 In vitro cytotoxicity of pure NDV and HA-TC-NDV at different concentrations ($n = 3$, mean + SD, $p \leq 0.05$)

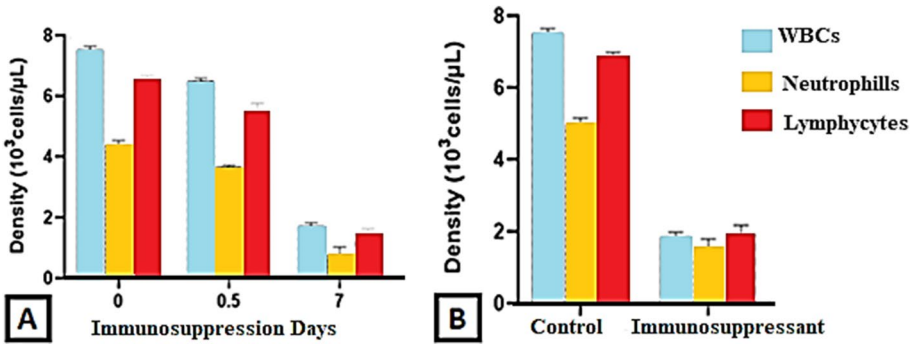

Fig. 4 Immunosuppression in rats at day 7: Graph **A** represents the mean of WBC, lymphocyte and neutrophil count on day 0, 0.75, and 7 in immunosuppressed animals. Graph **B** shows the complete protocol's mean WBC, lymphocyte and neutrophil count of control and immunosuppressed animals post cyclophosphamide treatment ($n = 10$, mean + SD, $p \leq 0.05$)

Physiological analysis of tumor growth

All animals' mean tumor volume and mean body weight was recorded every 7th day for 8 weeks following tumor implantation. The body weight decreased significantly in the CC group compared to the control group, but in the group receiving HA-TC-NDV (group 4), the loss of body weight was less than the group receiving pure NDV only (group 3). Mean body weight for group 1 (control) was 160 + 0.03 g which increased up to 240 + 0.01 g (20%) till the end of the experiment. For group 2 (CC group), it was 160 + 0.04 g which decreased up to 120 + 0.02 g (25%) till the end of the investigation. For group 3 (pure NDV), it was 160 + 0.02 g which decreased up to 135 + 0.03 g (15.62%) till the end of the experiment, for group 4 (HA-TC-NDV) was 160 + 0.02, which decreased up to 150 + 0.01 g (6.25%) till the end as depicted in Fig. 5A.

The mean tumor volume radically increased from 85 + 0.02 to 230 + 0.03 mm^3 from week one till week 8 in group 2 (cervical cancer). Group 3 (pure NDV) was treated with NDV after 10 days of tumor implantation at MOI of 12/week for 2 months, and tumor volume changed from 60 + 0.01 to 110.6 + 0.03 mm^3 till the 5th week, after which a sudden increase in tumor volume was observed that reached up to 178 mm^3 till 8th week. Tumor volume in group 4 that received HA-TC-NDV treatment was

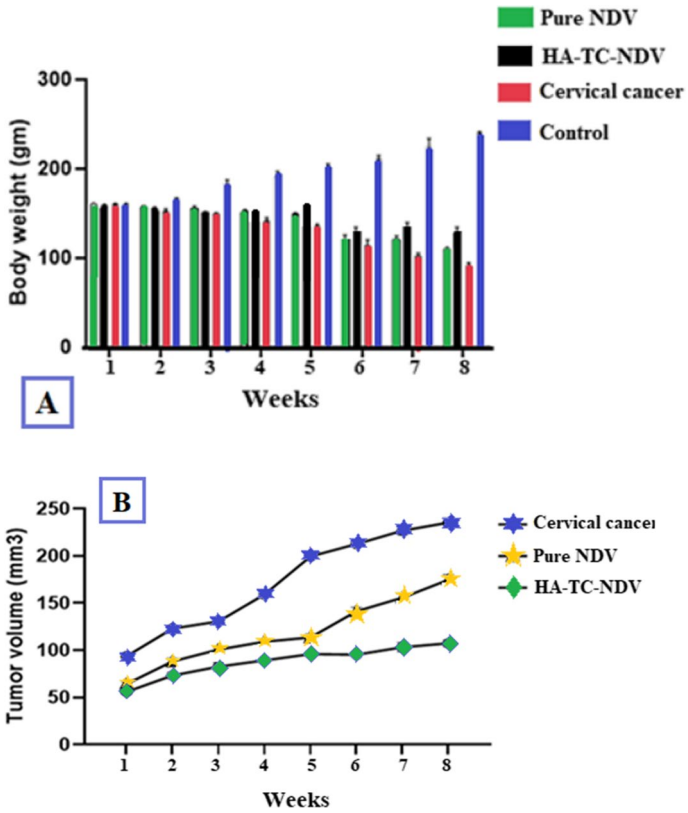

Fig. 5 Body weight (**A**) and tumor volume (**B**) in rat model after xenograft implantation of HeLa cells in pure NDV and HA-TC-HDV-treated groups

$50 + 0.02$ to $101.5 + 0.01$ mm^3, which is significantly smaller when compared to group 3 treated with pure NDV ($n = 10$) as shown in Fig. 5B.

Hematological parameters

The RBC, WBC and platelet profiles were analyzed in the blood of the CC and treatment groups. HA-TC-NDV nanoformulation showed a better RBC count of $4.9 \pm 0.24 \times 10^{12}$/L as compared to pure NDV ($2.96 \pm 0.32 \times 10^{12}$/L) and CC group ($3.39 \pm 0.20 \times 10^{12}$/L) RBC count. A decrease in hemoglobin (Hb) was evident in the disease group at 7.1 ± 0.15 g/dL compared to the pure NDV and HA-TC-NDV groups with Hb of 7.5 ± 0.25 g/dL and 9.1 ± 0.71 g/dL, respectively. Hematocrit of the HA-TC-NDV treatment group was $33.16 \pm 1.63\%$ with MCV at 72.5 ± 0.41 fl as compared to the pure NDV group with $30.93 \pm 2\%$ hematocrit and 87.64 ± 0.73 fl MCV and CC group with $30.72 \pm 2.1\%$ hematocrit and 98.7 ± 0.39 fl MCV. RBC morphology was macrocytic in CC, which was normal in all other groups. WBC count in HA-TC-NDV and pure NDV treatment group were within the normal range of $4.5–11 \times 10^3$/μL compared to the CC group with a WBC count of $32.1 \pm 2.5 \times 10^3$/μL. Neutropenia and lymphocytosis were profound in the CC group with $16 \pm 1.4\%$ neutrophil and $94 \pm 3.1\%$ lymphocyte count, respectively, while these counts were better in the pure NDV treatment group with $20 \pm 1.33\%$ neutrophils and $70 \pm 3.61\%$ lymphocyte. HA-TC-NDV showed even better neutrophil and lymphocyte profiles with $23 \pm 3.12\%$ and $59 \pm 2.52\%$ neutrophil and

lymphocytes, respectively, while WBC morphology was abnormal in pure NDV and HA-TC-NDV groups. No significant difference in platelet count was observed in all groups. The liver and renal function tests did not exhibit any considerable hepatotoxicity and renal toxicity across all groups ($n = 10$), as shown in Table 2.

Biochemical tests

To evaluate oxidative stress, the level of the antioxidant enzymes in serum samples of CC group and treatment group was quantified and then compared with the control group, as shown in Fig. 6. The MDA level in the CC group was 88.56 + 0.02 µmol/L, which decreased to 41.21 ± 0.02 and 39 ± 0.01 µmol/L in the pure NDV and HA-TC-NDV treatment group. The GSH level was 0.30 ± 0.02 mmol/L in the CC tumor model, which was reduced to 0.14 ± 0.01 and 0.11 ± 0.01 mmol/L in NDV and HA-TC-NDV groups, respectively. SOD level in the disease group was 184 ± 0.01 U/mL, while NDV and HA-TC-NDV groups had levels decreased to 139 ± 0.01 and 121 ± 0.02 U/mL, respectively.

Table 2 Complete blood profile with renal and hepatic parameters in control, CC, pure NDV and HA-TC-NDV groups

Parameters	Control ($n = 10$)	Cervical cancer ($n = 10$)	Pure NDV ($n = 10$)	HA-TC-NDV ($n = 10$)	Range (unit)
RBC profile					
RBC count	5.8 ± 0.41	3.39 ± 0.20	2.96 ± 0.32	4.9 ± 0.24	4–5.9 × 10^{12}/L
Hemoglobin	15 ± 0.27	7.1 ± 0.15	7.5 ± 0.25	9.1 ± 0.71	12–16 × g/dL
Hematocrit	45.98 ± 1.20	30.72 ± 2.1	30.93 ± 2.0	33 ± 1.63	35–50%
MCV	47 ± 0.61	98.7 ± 0.39	87.64 ± 0.73	72.5 ± 0.41	40–60 fl
MCH	25 ± 0.51	18.5 ± 0.35	15.3 ± 0.6	20.3 ± 0.38	21–31 pg
MCHC	30 ± 0.47	48.4 ± 0.56	45.72 ± 0.45	42.3 ± 0.51	30–39%
Hemolysis	2 ± 0	10.67 ± 0.3	24 ± 0.3	16.2 ± 0.4	0%
RBC morphology	Normal	Macrocytic	Normal	Normal	Normal
WBC profile					
WBC count	7.4 ± 1.31	32.1 ± 2.5	9.0 ± 1.51	10.2 ± 0.51	4.5–11.0 × 10^{3}/µL
Neutrophils	22 ± 1.86	16 ± 1.4	20 ± 1.33	23 ± 3.12	21–57%
Lymphocytes	50 ± 3.0	94 ± 3.1	70 ± 3.61	59 ± 2.52	49–82%
Monocytes	1.63 ± 0.51	9.7 ± 0.2	2.9 ± 0.51	2.68 ± 0.4	1.7–4.3%
Eosinophils	2.31 ± 0.22	15 ± 0.17	3.9 ± 0.16	1.94 ± 0.64	0–3%
Basophils	2.30 ± 0.17	0.22 ± 0.32	0.7 ± 0.31	2.14 ± 0.31	0–3%
WBC morphology	Normal	Abnormal	Abnormal	Abnormal	Normal
Platelet profile					
Count	380,000 ± 0.39	470,000 ± 0.47	320,000 ± 0.43	355,000 ± 0.36	150,000–450,000 µL
Morphology	Normal	Normal	Normal	Normal	Normal
Kidney function test					
BUN	16.23 ± 0.13	30 ± 0.44	26 ± 1.05	19 ± 0.29	18–29 mg/dL
Creatinine	0.1 ± 0.02	0.35 ± 0.18	0.5 ± 0.19	0.35 ± 0.11	0.1–0.4 mg/dL
Liver function test					
ALT	19 ± 4.1	50 ± 3.15	25 ± 4.12	27 ± 4.72	4.1–36 U/L
AST	13 ± 2.12	45 ± 3.4	30 ± 3.54	25.66 ± 4.17	8.1–33 U/L
ALP	15 ± 1.67	47.1 ± 3.1	31 ± 2.27	36.33 ± 4.6	4.1–40 U/L

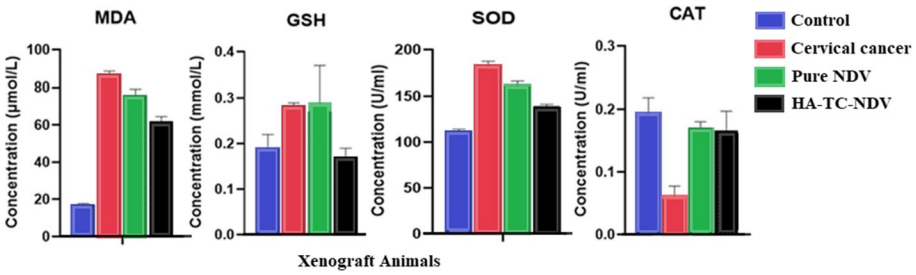

Fig. 6 Antioxidant enzyme levels for MDA, GSH, SOD, and CAT at the end of the experiment in the CC group, NDV and HA-TC-NDV treatment groups

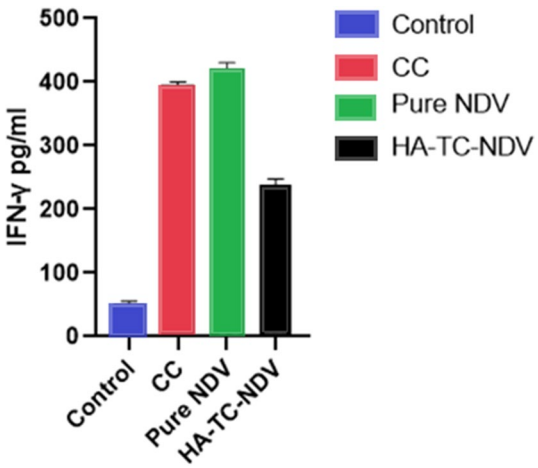

Fig. 7 NK cell activity analysis (IFN-γ levels) in cervical cancer (CC) vs NDV and HA-TC-NDV-treated groups

CAT level was 0.07 ± 0.02 U/mL in the CC group while it was slightly increased to $0.17 + 0.02$ and $0.22 + 0.02$ U/mL in both treatment groups, respectively ($n = 10$), as shown in Fig. 6

Ex vivo NK cell activity assay

Evaluation of ex vivo NK cell activity from venous blood showed that NK activity was 400 pg/mL in group CC animals, 422 pg/mL in animals treated with pure NDV, while in animals treated with HA-TC-NDV, it was significantly reduced to 240 pg/mL, which is much lower than the CC and pure NDV treatment group ($n = 10$) as shown in Fig. 7

Histopathological analysis

Histopathological analysis of cervical cancer xenograft tumors and treatment groups was performed. Tissue from significant organs and tumors was sectioned and stained with hematoxylin and eosin dye. The tumor-bearing CC animal groups showed significantly large nuclei in malignant cells with scanty cytoplasm and irregular shape, while some places showed invasion to the neighboring stroma. The CC groups showed significant metastatic lesions (Fig. 8a, A2: brain, B2: kidney, C2: heart, D2: lungs, E2: liver, F1–F2: before and after tumor area) while tissue morphology was normal in the control group (Fig. 8a, A1: brain, B1: kidney, C1: heart, D1: lungs, E1: liver) as shown in Fig. 8a.

Oncolytic effect was dominant in pure NDV (Fig. 8b, A3: brain, B3: kidney, C3: heart, D3: lungs, E3: liver) group as compared to HA-TC-NDV treatment group (Fig. 8b, A4: brain, B4: kidney, C4: heart, D4: lungs, E4: liver). Syncytium formation, a hallmark of oncolytic viral infection of cells, can be seen in F3 and F4 for pure NDV treatment and HA-TC-NDV treatment groups, respectively.

Immunohistochemistry

Immunohistochemical staining for TNF-α, COX-II and NFκB antibodies was performed on xenograft tumors (E) and other major organs, including brain, heart, liver and lungs from control (A1–A12) xenograft CC tumor (B1–B12) as shown in Fig. 9a, HA-TC-NDV (C1 to C12) and pure NDV (D1–D12) treatment group as shown in Fig. 9b. Analysis of obtained images exhibited high expression of TNF-α, COX-II and NFκB in nuclei and cytoplasm of tumor cells on day 16, as shown in Fig. 10. Among all cancer groups, the highest expression was observed in lung and liver tissues, confirming metastasis to these sites. Cytoplasmic COX-II and TNF-α staining and nuclear staining of NFκB showed increased expression in the CC group liver (B7–B9) and lungs (B10–B12). Staining of tumor tissue from HA-TC-NDV shows syncytia formation (E1–E3), depicting a strong oncolytic activity of nanoformulation in tumor cells, as shown in Fig. 10. Strong staining in lungs for the HA-TC-NDV group represents high targeting capacity of nanoformulation not only against tumor sites, but also against metastatic lesions anywhere else in the body.

ELISA

In addition to cancer markers TNF-α, COX-II and NFκB, the expression of BCL-2, BAX, cleaved Caspase-3 and cleaved PARP proteins in the systemic circulation of xenograft animals and treatment groups was also measured by performing ELISA. A significant increase in cleaved Caspase-3, Bax and cleaved PARP was observed, while the expression of BCL-2 was reduced in pure NDV and HA-TC-NDV treatment groups compared to the CC tumor group, as shown in Fig. 11(A), which shows potent oncolytic effect. The expression of Bax decreased from 13.87 ± 0.21 to 3.39 ± 0.18, cleaved PARP and cleaved Caspase-3 decreased from 845 ± 0.22 to 660 ± 0.35 and 224 ± 0.16 to 110 ± 0.19, while BCL-2 level increased from 52 ± 0.09 to 69.3 ± 0.25 in control and CC xenograft group. In pre NDV and HA-TC-NDV treatment groups, Bax expression increased from 3.39 ± 0.18 to 16.89 ± 0.13 and 36.6 ± 0.21, BCL-2 expression decreased from 69.3 ± 0.25 to 40.9 ± 0.22 and 27 ± 0.16, cleaved PRP increased from 660 ± 0.35 to 1156 ± 0.11 and 1367 ± 0.21, cleaved Caspase-3 had much increased from 110 ± 0.19 to 1111 ± 0.14 and 1653 ± 0.26, respectively, as shown in Fig. 11(A)

The expression of TNF-α increased from 901 ± 0.25 pg/mL (control) to 3200 ± 0.12 pg/mL (cancer model) and then decreased from 3200 pg/mL to 1760 ± 0.31 and much reduced 1120 ± 0.18 pg/mL in NDV and HA-TC-NDV group, respectively. NFκB and COX-II expression increased from 0.4 ± 0.14 pg/mL and 0.8 ± 0.25 (control) to 1.92 ± 0.31 pg/mL and 1.90 ± 0.22(cancer model). This expression decreased from 1.92 ± 0.31 to 0.76 ± 0.22 and 0.52 ± 0.07 pg/mL for NFκB and from 1.90 ± 0.25 to 0.81 ± 0.32 and 0.7 ± 0.30 for COX-II in NDV and HA-TC-NDV group, respectively as shown in Fig. 11(B). The expression of all interactive proteins

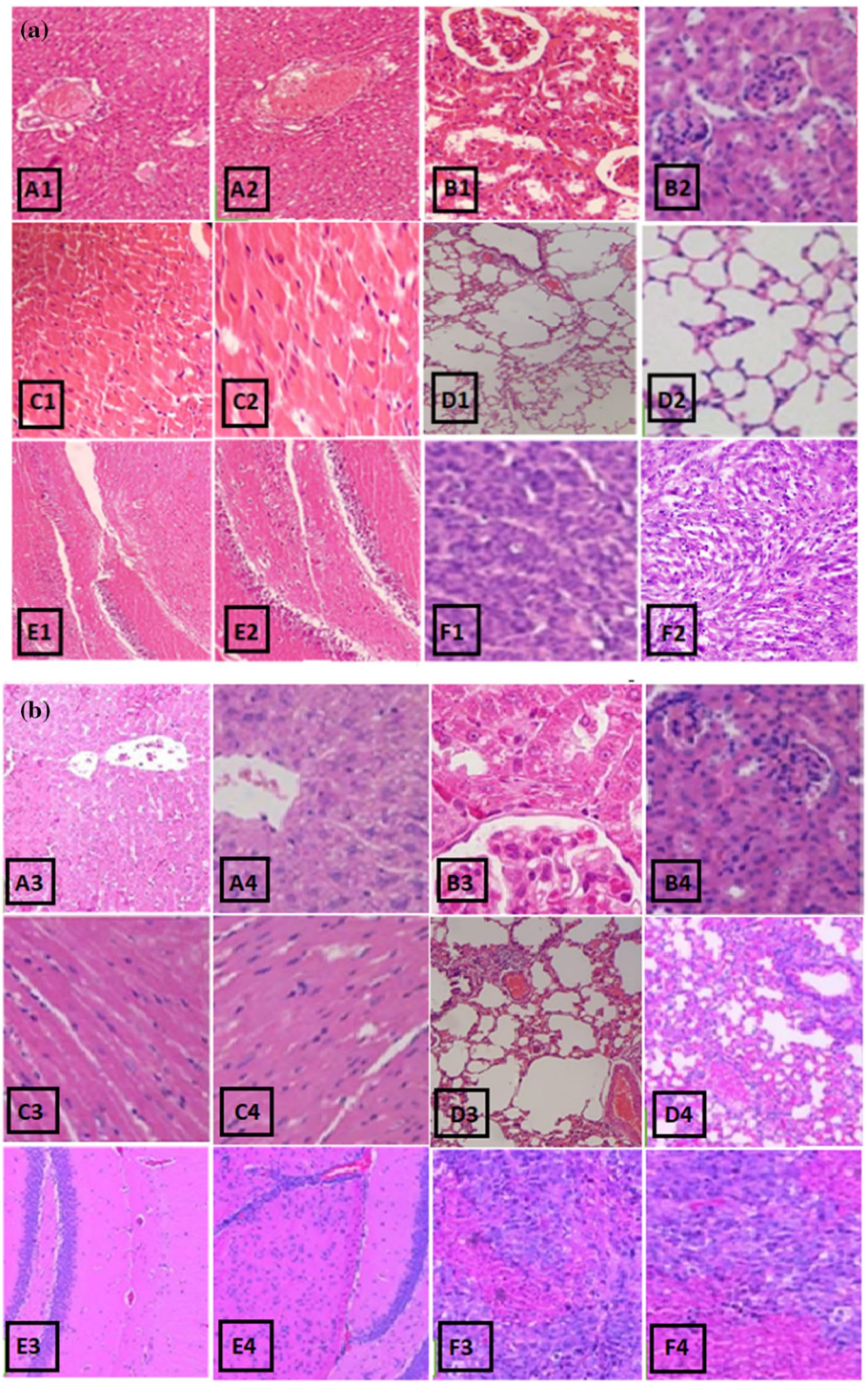

Fig. 8 **a** Histopathology of tissues from control and cervical cancer (CC) xenograft group: Control group (A1: brain, B1: kidney, C1: heart, D1: lung, E1: liver), CC group (A2: brain, B2: kidney, C2: heart, D2: lung, E2: liver. F1 and F2 show tumor histopathology from flank tissues of control and xenograft model, respectively. **b** Histopathology of tissues from pure NDV group and HA-TC-NDV treatment group: pure NDV group (A3: brain, B3: kidney, C3: heart, D3: lung, E3: liver), HA-TC-NDV group (A4: brain, B4: kidney, C4: heart, D4: lung, E4: liver). F3 and F4 show tumor histopathology with irregular cellular arrangements in both groups

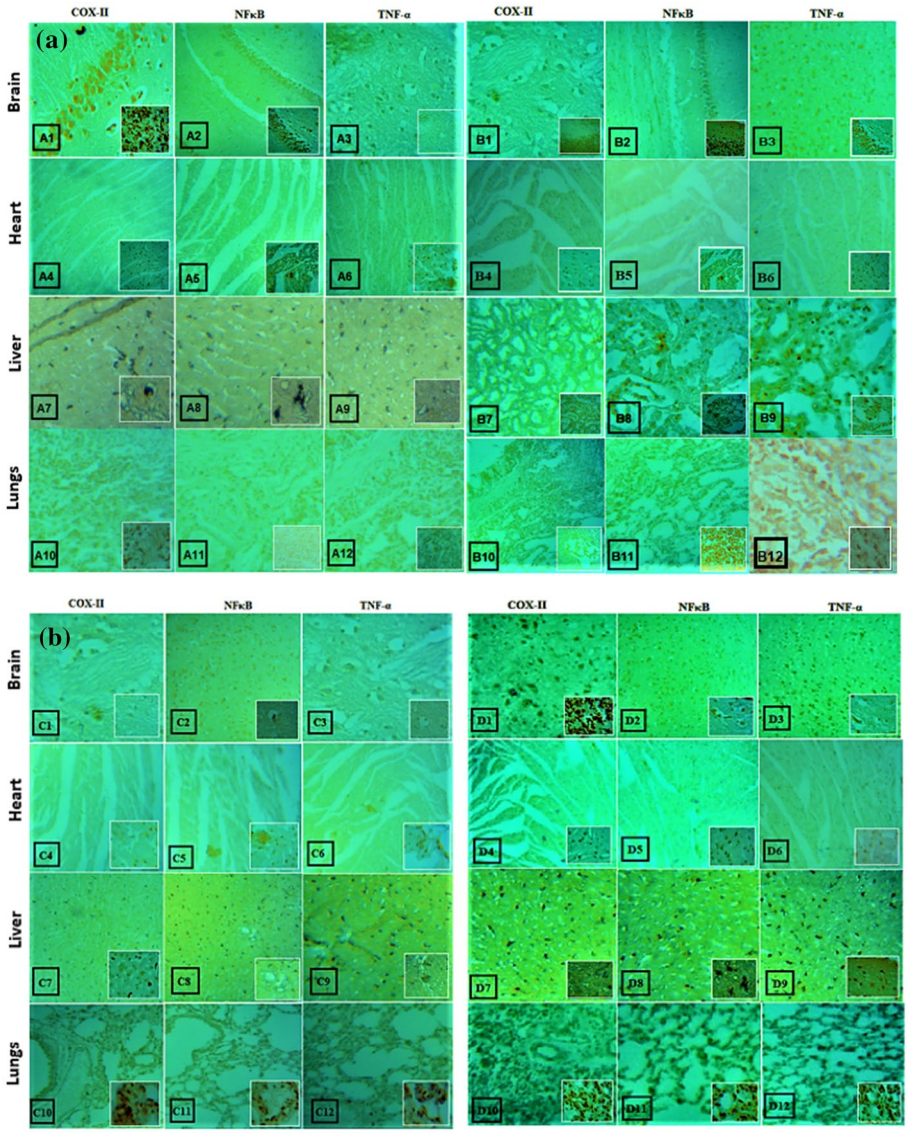

Fig. 9 **a** Immunohistochemical staining for COX-II, NFκB and TNF-α in control (A1-A12), CC (B1-B12) group. **b** Immunohistochemical staining for COX-II, NFκB and TNF-α in HA-TC-NDV (C1-C12) and pure NDV treatment (D1-D12) group

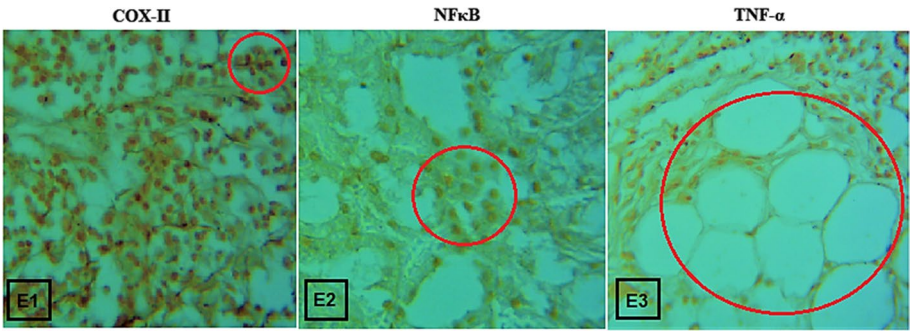

Fig. 10 Immunohistochemical staining for COX-II, NFκB and TNF-α in tumor tissues from HA-TC-NDV group. Red circles indicate syncytia formation

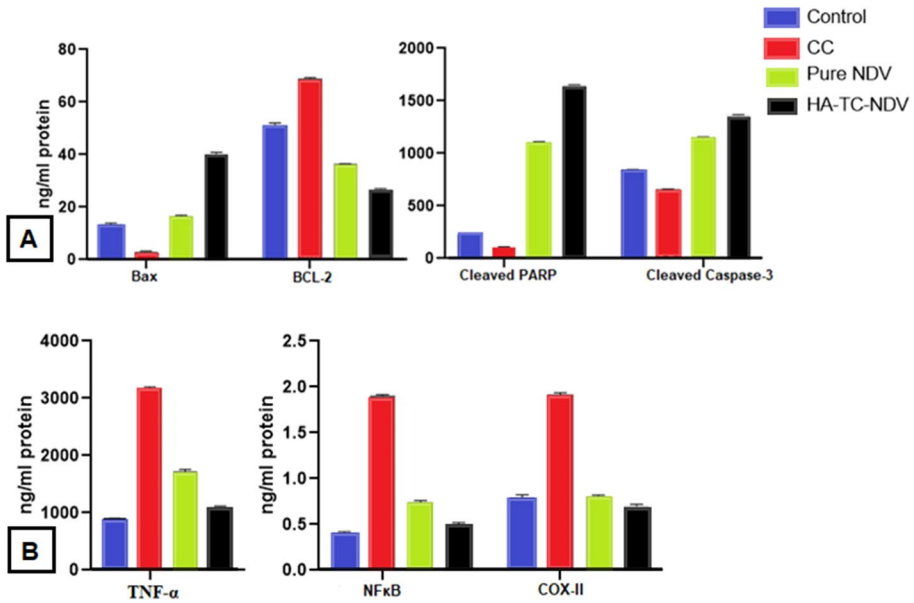

Fig. 11 **a** RT-PCR showing expression of Bax, BCL-2, cleaved PARP and cleaved Caspase-3 in control, CC, pure NDV and HA-TC-NDV treatment group. **b** RT-PCR showing expression of TNF-α, COX-II and NFκB in control, CC, pure NDV and HA-TC-NDV treatment group

involved in tumorigenesis had increased in the diseased group compared to the control and significantly decreased in the treatment group. It can be seen that the suppression effect was more pronounced in the HA-TC-NDV group, which shows a better oncolytic profile of encapsulated NDV as compared to pure NDV.

RT-PCR for viral quantification

Viral quantification analysis by RT-PCR from various organs and tumors showed that no virus was detected in the brain and heart of pure NDV and HA-TC-NDV treatment groups. A significantly higher copy number was observed in tumor tissues from animals treated with HA-TC-NDV compared to the pure NDV treatment group. Viral copy number detection in the liver and lungs of both groups shows that NDV accumulated in the lungs and liver probably because of tumor metastasis to these sites, as depicted in immunohistochemical staining. The highest viral copy number in the HA-TC-NDV group shows better release, accumulation and sustained virus release in targeted tumors, as shown in Fig. 12.

In vitro release of NDV from nanoformulation

The release of NDV from nanoformulation compared to pure NDV in phosphate PBS at pH 6.8 confirmed sustained virus release. Per our findings, pure NDV was released within 8 h, while NDV from nanoformulation was released for up to 48 h, as shown in Fig. 13, supporting our hypothesis of controlled and sustained virus release from nanoformulation.

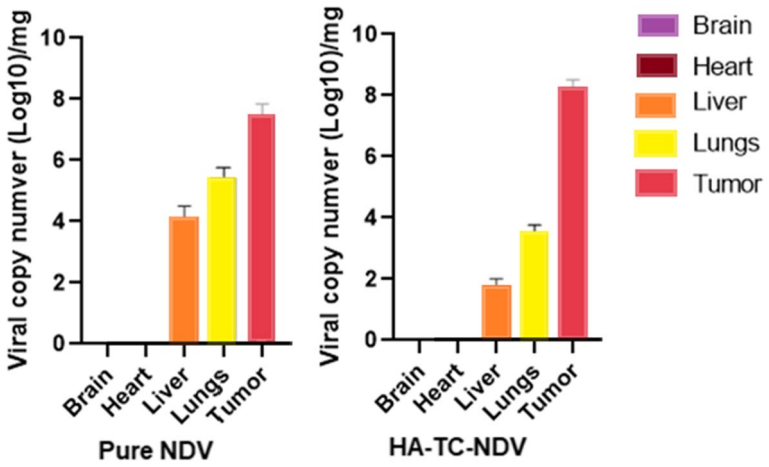

Fig. 12 Expression of viral copy number in pure NDV and HA-TC-NDV groups

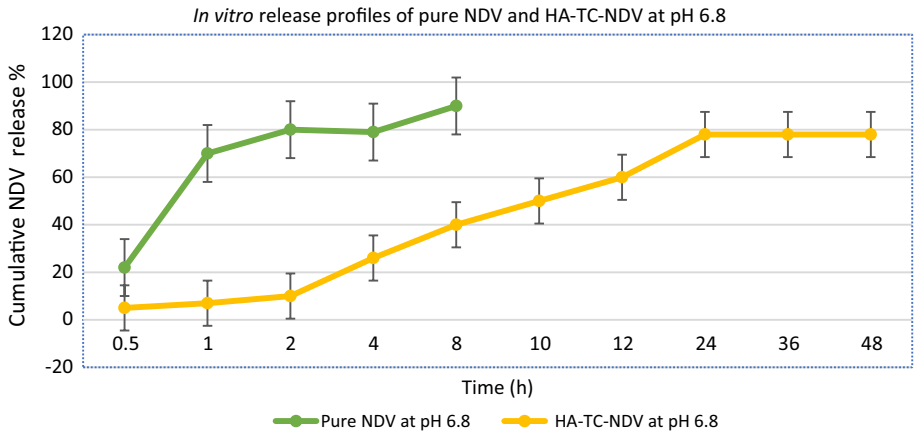

Fig. 13 In vitro release profile of pure NDV and HA-TC-NDV in PBS at pH 6.8

Discussion

Oncolytic Newcastle disease virus, an avian influenza virus, is selectively pathogenic and does not cause serious harm in humans. As reported, in humans NDV may cause conjunctivitis (eye infection, also called pink eye), mild flu-like symptoms and in some cases laryngitis (swelling of voice box). NDV strain, Lasota belongs to lentogenic (less pathogenic strain) class and has proven potent oncolytic potential in humans (Schirrmacher and Fournier 2009). One of the major setbacks faced in this treatment regimen is the immune neutralization of the virus as soon as the virus enters the body, which is basically initiated by natural killer (NK) cells and macrophages, ultimately leading to a strong antiviral innate and adaptive immune response against the virus (Burman et al. 2020).

The current research aimed at formulation of a nano-delivery system for targeted delivery and sustained release of Newcastle disease virus in cervical cancer while masking the virus from immune neutralization in vivo. For this purpose, thiolated chitosan (TC) nanoformulation was chosen as drug delivery system owing to its mucoadhesive, biocompatible and biodegradable properties and CD44 targeting was chosen due to overexpression of CD44 receptors on solid cancers. Targeted delivery of the NPs was

achieved by surface functionalizing TC nanoparticles with hyaluronic acid which is suitable candidate for this receptor (Puluhulawa et al. 2022). Figure 14 shows the illustration of immuno-oncolytic effect of NDV-loaded thiolated chitosan nanoparticles by CD44-mediated active targeting.

The size of virus encapsulated nano-delivery system was calculated to be 286.9 nm with a zeta potential of 18.1 mV and PDI of 0.241 which makes them ideal for tumor targeting as particle size under 300 nm are favorable to squeeze through leaky tumor vasculature and show longer retention time in tumor microenvironment (TME). Moreover, our nanoformulation exhibited sustained release of virus for up to 48 h as compared to pure NDV which was released in 8 h (Baranov et al. 2021). These findings are in accordance with another study in which mucoadhesive ThCs nanoparticles loaded with curcumin with a diameter between 200 ± 50 nm and zeta potential of 11–38 mv were tested against vaginal fluid simulant. The results showed a sustained release of curcumin for up to 3 days, confirming a significant decline in viral clearance, greater permeation and mucoadhesive nature of ThCs nanoparticles (Hasanifard et al. 2017). After encapsulation of the virus followed by a thorough characterization, viral titer was determined in nanoparticles by MOI and TCID50. The oncolytic potential of HA-TC-NDV was directly proportional to MOI of the virus and was greater than pure NDV at same MOI. $TCID_{50}$ for HA-TC-NDV and pure NDV was 4.1 and 6.0, respectively, which again depicts higher oncolytic potential of nanoparticle-encapsulated NDV, most probably because of very high over expression of CD44 on metastatic solid cancers resulted in targeted delivery of the virus. These findings are in accordance with results reported by Naseer et al., who used vaccine strain of oncolytic measles virus (OMV) encapsulated in HA-coated thiolated chitosan nanoparticles for targeted delivery in prostate cancer PC3 cells. The reported $TCID_{50}$ for HA-TC encapsulated OMV was 3.52 while that of pure OMV was 5.1 (Naseer et al.

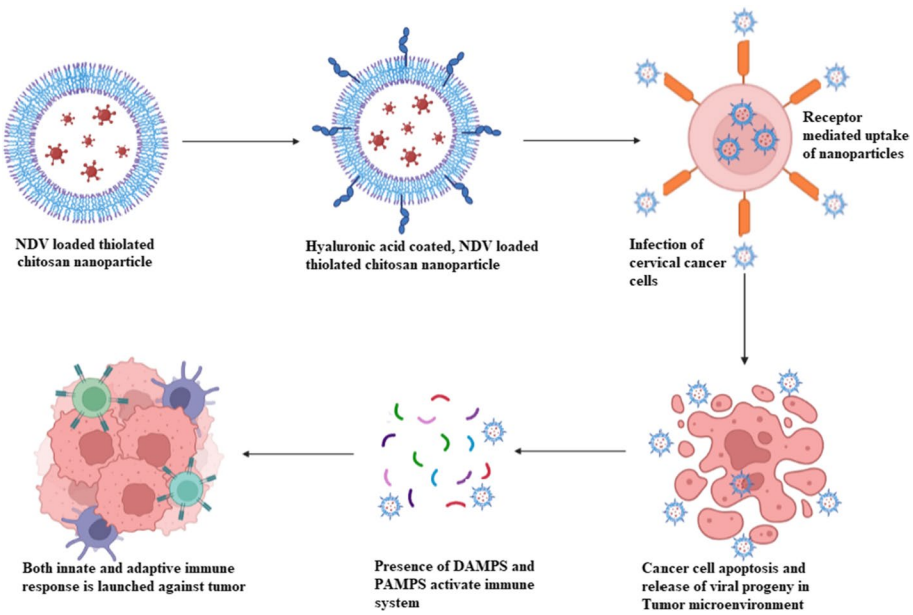

Fig. 14 Schematic view of NDV encapsulation in HA-TC NPs and immune activation by HA-TC-NDV in tumor microenvironment

2023). The same trend was observed while testing the in vitro anticancer potential of HA-TC-NDV and pure NDV in HeLa cells, since the MTT cytotoxicity assay showed that at a concentration of 15 µg/mL the cytotoxicity of HA-TC-NDV was slightly lower than that of pure NDV (sustained release); however, with increasing concentration, the oncolytic potential of HA-TC-NDV substantially increased as compared to pure NDV, confirming enhanced uptake of nanoparticle. These findings are supported by our previous study in which cisplatin-loaded HA-coated thiolated chitosan nanoparticles showed enhanced cytotoxic effect in HeLa cells (Kousar et al. 2023).

Immunocompetent Wister rats with an intact immune system were used instead of Balb/c mice for the in vivo analysis, as we believe that the presence of a normal immune system is a crucial part of the actual tumorigenic process, since certain cells such as tumor-associated fibroblasts and tumor-associated macrophages (M2 macrophages) play a key role in tumor progression. Prior to tumor implantation, immunosuppression was achieved by using cyclosporin, ketoconazole, complete WBC profiling later confirmed immune suppression. Complete WBC, RBC and platelet profile showed that the treatment groups had better outcomes of hematological parameters as compared to CC group and HA-TC-NDV group had most of the parameters falling under desirable range which is attributed to confinement of the virus to TME. Measurements of serum antioxidant enzymes in CC and treatment groups showed decrease in oxidative stress in HA-TC-NDV group as compared to pure NDV and CC group. Ex vivo NK cell activation was measured by quantifying IFN-γ which is released by NK cells activation. IFN-γ level of 240 pg/mL in HA-TC-NDV-treated group was significantly lower ($p < 0.05$) as compared to 422 pg/mL in pure NDV-treated group hence showing successful masking of the oncolytic NDV from immune system and the ultimate enhancement of the oncolytic effect. As reported by an earlier study, immune competent C57BL/6 mice bearing TC-1 cells indued tumors, when treated with oncolytic reovirus loaded in mesenchymal stem cells (MSCs) showed enhanced uptake and oncolytic potential as compared to naked reovirus (Seyed-Khorrami et al. 2021).

Following hematological profiling, histopathological analysis was performed to verify the effect of HA-TC-NDV nanoformulation on all major organs and tumors. Histopathological studies showed that CC group and pure NDV-treated group had metastatic lesions in liver and lungs; whereas this effect was not much evident in HA-TC-NDV treatment groups. Histopathological staining of tumors showed enhanced apoptotic effect with syncytia formation, which is a hallmark of oncolytic viral infection of tumors (Burton and Bartee 2019). Immunohistochemistry analysis for TNF-α, COX-II and NFƘB as marker of tumor-associated inflammation and enhanced tumor progression showed a relatively higher expression of these markers in lungs and liver of the CC and pure NDV treatment showing metastasis to these sites as compared to HA-TC-NDV group. As compared to tumors from CC and treatment groups, decrease in expression of NF-ƘB, TNF-α and COX-2 was significantly higher ($p < 0.05$) in HA-TC-NDV treatment group. The results further support the previously reported infection of HeLa cells with oncolytic NDV altered NF-kB expression, demonstrating its crucial role in NDV-mediated oncolysis in cervical cancer (Chen et al. 2021). These findings are also supported by ELISA outcomes for TNF-α, NF-ƘB and

COX-2 which showed a substantial decrease in expression of these genes in HA-TC-NDV group as compared to CC and pure NDV group ($p < 0.05$).

Furthermore, ELISA analysis showed that increase in the expression of proapoptotic Bax, cleaved PARP and cleaved Caspase-3 while decrease in BCL-2 (anti-apoptotic) expression was much more significant ($p < 0.05$) in HA-TC-NDV treatment group as compared to pure NDV and CC group. Similar enhanced expression of cleaved Caspase-3 and cleaved PARP was documented in NDV-mediated apoptosis and inhibition of migration in oral cancers (Morla et al. 2019). Another study reported decrease in BCL-2 and increase in Bax expression when TRAIL armed oncolytic NDV was evaluated for lung cancer animal models (Hu et al. 2018).

Quantification of viral copy number in the tumor and some major organs provided evidence of viral spread and accumulation in vivo. A higher viral copy number of oncolytic NDV was observed in lungs and liver in pure NDV treatment group, which is in consistent with findings reported by another study where a high retention of NDV expressing human-IL12 was observed in breast cancer tumors along with accumulation of the virus in lungs and liver (Mohamed Amin et al. 2019). On the other hand, accumulation of the virus in the tumor was highest in the HA-TC-NDV group and substantially lower ($p < 0.05$) in the lungs and liver owing to targeted virus delivery.

Conclusion

This research supports the hypothesis that encapsulation of oncolytic NDV in thiolated chitosan nanoparticles for CD44 targeted delivery improves oncolytic effect of the virus. This novel virus-loaded nanoformulation showed improved hematological profiles in xenograft models with better cytopathic effect at lower dosage of the virus and improved release of the virus for up to 48 h which will increase bioavailability of the virus in TME. The better oncolytic effect of nanoformulation-loaded NDV as compared to pure NDV was further established by hematological, physiological, histopathological and antioxidant parameters. The expression of TNF-α, COX-II, and NFκB was confirmed by immunohistochemical and ELISA-based analysis. Moreover, viral quantification showed enhanced accumulation of the virus at tumor site in nanoformulation-treated animal group as compared to pure NDV-treated group. Thereafter, it can be concluded that the thiolated chitosan loaded, HA coated and CD44 targeted nanoformulation is a promising carrier of oncolytic viruses with reduced immune clearance of the virus from the body and better oncolytic potential in cervical cancer.

Methods

Materials

Acetonitrile and methanol (HPLC grade) were purchased from Adnan Traders, Rawalpindi. Normal saline, distilled water and phosphate buffer saline were prepared using a Milli-Q purification system (Millipore, Billerica, MA, USA). Low molecular weight chitosan (50–190 kDa, 70–80% deacetylation) and tripolyphosphate polyanions (TPP) were purchased from Scharlau (Germany). Matrigel, Triton X-100, disodium EDTA solution, xylocaine, ketamine, ketoconazole, amoxicillin, cyclosporine and cyclophosphamide injections were obtained from Shifa International Hospital Pharmacy, Islamabad, Pakistan. HeLa human cervical cancer cell line were provided by Dr Saeed Khan, Dow

University of Health Sciences, Ojha Campus, Karachi. Cell culture medium Dulbecco's modified Eagle medium (DMEM-Gibco), fetal bovine serum (FBS-Gibco), Penstrep (Penicillin Streptomycin-Gibco), trypan blue (Gibco), trypsin (Gibco), sodium bicarbonate, and sodium pyruvate were purchased from Biolife Technologies, Islamabad, Pakistan. A rodent diet was prepared in the National University of Sciences and Technology's animal house in Islamabad, Pakistan.

Synthesis of HA-TCs-NDV nanoformulation

By using thiolated chitosan, NDV-loaded nanoformulation was synthesized with the ionic gelation method and green synthesis protocol, as mentioned in the previously published study, with a slight modification (Kousar et al. 2023). To a 5 mL (0.1 mg/mL) solution of thiolated chitosan, a half dose of NDV (TCID of single dose $= 3 \times 10^5$) was added dropwise while constantly stirring at 540 rpm on a magnetic stirrer. Afterwards, 0.10 mL of TPP (tripolyphosphate) was added as a cross-linker to facilitate nanoparticle synthesis. Afterwards, sonication was done by using probe sonicator at 0.3 mA for 1 min of ultrasound and a pause of 30 s after each pulse. Following sonication, 2 mL of HA was added at 0.5 mg/mL concentration for surface functionalization of NDV-nanoformulation (HA-TC-NDV) while constantly stirring for 10 min (mins) at 540 rpm on the magnetic stirrer. The final solution was centrifuged, lyophilized and stored at 4 °C until required (Naseer et al. 2022).

Physiochemical characterization of HA-TC-NDV

To analyze physiochemical characteristics and for morphological assessment of HA-TC-NDV, further analysis was performed according to the protocols mentioned in our previous study. SEM and TEM were performed to evaluate surface morphology, Zeta analysis was carried out to assess the size, homogeneity, and surface charge; FTIR, and XRD were employed to ensure encapsulation and analysis of the functional group as mentioned in our previous study (Kousar et al. 2023; Naseer et al. 2023).

Cell culture

HeLa cells were cultured in a T25 flask in recommended cell culture media DMEM and the 2 mM L-glutamine, 1 mM sodium pyruvate, 1.5 g/L sodium bicarbonate, with 10% FBS and 0.5% Penstrep at 37 °C with 5% CO_2 and 95% air. Cells were used for the experimental purpose in the exponential growth phase and after reaching 75–80% confluency (Zani et al. 2023).

$TCID_{50}$

The viral titer of the nanoformulation was measured by determining $TCID_{50}$ using the Reed–Muench protocol. A 1:10 titer solution of lyophilized HA-TC-NDV was prepared in 10 µL PBS buffer at a dilution ratio of 10^{-3} to 10^{-12} (pH = 7.2). HeLa cells were cultured in 96-well plate at a density of 0.5×10^4 cells/well and incubated at 37 °C and 5% CO_2. The following day, cells were treated with $10\times$ serial dilution of HA-TC-NDV and were again incubated under the above mentioned conditions. Cells were analyzed at 7 p.d.i using an inverted microscope, and the resulting titer was reported as TCID50 or endpoint dilution assay following Reed and Muench protocol. HeLa cells treated with pure NDV served as a

positive control, while cells treated with DMEM only served as a negative control. The concentration of HA-TC-NDV in one $TCID_{50}$ equals a viral titer that would infect 50% of cells (Ramakrishnan et al. 2016) (Lei et al. 2021).

MOI

HeLa cells were cultured in 6-well culture plates at a seeding density of 2×10^6 cells/10 cm^2. Cells were infected with Pure NDV and HA-TC-NDV at MOI of 0.1, 0.6, 1, 5, 8, 12, 18 and 20. The plates were incubated for 2 h to make the virus adhere to the cells. Following incubation, cells were washed with DMEM media twice to remove any unbound virus. Afterwards, cells were incubated at 37 °C with 5% CO_2 for 3 days (Fulber et al. 2021).

Trypan blue exclusion assay

The cytopathic effect of nanoformulation on HeLa cells was evaluated by trypan blue exclusion assay. Cells were grown in a 24-well plate at a seeding density of 13×10^4/well. The next day, the supernatant was removed, and cells were harvested using 0.25% Trypsin–EDTA. DMEM media was added to stop trypsin activity, and the cell palette was collected by centrifugation at 800 rpm for 4 min. After washing with PBS, the cells were suspended in 1 mL of fresh medium. Afterwards, 50 µL of cell suspension was mixed with 50 µL of 0.4% trypan blue dye and incubated for 2 min (Madar et al. 2022). Dead (blue) and living cells (white) were counted using a hemacytometer under a phase contrast inverted microscope. Cell viability percentage was calculated using the below-mentioned formula, while % cytotoxicity was calculated by subtracting % cell viability from 100:

$$\% \text{ Cell viability} = \frac{\text{No. of viable cells/mL}}{\text{Total number of cells/mL}} \times 100.$$

MTT cytotoxicity assay

The cytotoxicity potential of HA-TC-NDV was evaluated using an MTT cytotoxicity assay. MTT assay is a colorimetric assay based on the ability of living cells to convert water-soluble dye [3-(4,5-dimethylthiazol-2-yl)-2,5-diphenyltetrazolium bromide] into an insoluble formazan. HeLa cells were seeded in a 96-well plate at a cellular density of 1×10^6 in 100 µL/ well and incubated for 24 h. The following day media was refreshed, and cells were inoculated with various concentrations of HA-TC-NDV at MOI of 0.1, 0.6, 1,5,8,12, 18 and 20. Cells were allowed to incubate for 72 h. After incubation, 10 µL of MTT dye was added to the cells (at 0.45 mg/mL) and cells were incubated for 4 h. After 4 h, MTT dye was removed, and 100 µL of DMSO (dimethyl sulfoxide) was added to dissolve formazan crystals. Cell viability was analyzed using the following formula (Cao et al. 2021):

$$\text{Cell viability } (\%) = \frac{\text{O.D. of cells treated with drug/N.P.s} - \text{O.D. blank}}{\text{OD of control cells} - \text{OD of blank}} \times 100.$$

In vitro release of virus from NPs

For evaluating in vitro release of the NDV from nanoformulation, 0.1 g of lyophilized HA-TC-NDV was poured into a dialyzing membrane immersed in 50 mL PBS at 6.8 pH. This dissolution assembly was placed on a magnetic hotplate with constant stirring at

100 rpm at 37 °C. 1.5 mL of the sample was collected after time intervals of 0, 0.5, 1, 2, 4, 8, 10, 12, 24, 36, and 48 h and centrifuged at 10,000 g/min. Using a spectrophotometer, all samples were analyzed for release of NDV from NFs at 520 nm. The time duration for NDV release was plotted at *X*-axis, while the accumulative amount of released NDV was plotted at *Y*-axis to get the virus release curve (Loutfy et al. 2022).

In vivo antitumor potential

To test the efficacy of CD44, targeted HA-TC-NDV animal-based studies were performed to monitor the efficacy of pure NDV and HA-TC-NDV. For this purpose, 10–12 weeks old wistar rats weighing approximately 200–250 g were collected from the animal house of Atta-ur-Rahman School of Applied Biosciences (ASAB), National University of Science and Technology (NUST), Islamabad Pakistan, under the Ethical approval no. 04–2022-ASAB-01/01. Animals were kept at 25 °C with a 65% humidity environment. Water ad libitum and balanced food pallet was given to animals regularly with dark: light cycle of 12:12 h (Gu et al. 2021).

The following grouping was done for experimental analysis with 10 rats in each group:

Group 1: Control.

Group 2: Disease/cervical cancer (CC) group.

Group 3: Pure NDV treatment group.

Group 4: HA-TC-NDV treatment group.

Groups 3 and 4 received pure NDV and HA-TC-NDV at MOI of 5×10^3. Lyophilized HA-TC-NDV was reconstituted in 2 mL of PBS before administration.

Protocol for animal studies

Before starting an experiment, the animals were allowed to acclimatize for one week. NUST institutional Review Board reviewed the experimental protocol before the commencement of the investigation. Rats were divided into 4 groups containing 10 animals in each. One group served as a control group (buffer only), other three groups were tumor xenograft models. Among these three groups, one served as the tumor model (cervical cancer), and the other served as the treatment group for pure NDV and HA-TC-NDV (Mesas et al. 2022).

Immunosuppression Immunosuppression was achieved by administering Ketoconazole at 10 mg/kg through the oral route and intraperitoneal administration of cyclosporine at 30 mg/kg daily for one week. During the study, rats were also given 0.1 µg/mL of amoxicillin with drinking water. For the determination of the total white blood cells (WBCs), WBC profiling was performed by analyzing neutrophils and lymphocyte count to monitor immunosuppression at the beginning of the protocol (day-0), after 18 h (day-0.75) and after one week (day-7). After maximal immunosuppression was observed, Cyclophosphamide was administered to rats subcutaneously at 60 mg/kg on days 1 and 3 before the animals were injected with tumor cells. Blood samples were collected in a 1.5 mL heparinized tube from the rats' tail vein after lidocaine gel application sat the beginning of the experiment, at 18 h of day 1 and day 7 (Diehl et al. 2017). An automated hematology analyzer (VetScan HM-5; Abaxis Inc., Union City, CA, USA) was used for complete WBC profiling.

Tumor implantation The confluent monolayer of HeLa cells in T25 flask was trypsinized using 1 mL of 0.25% trypsin for detaching cells. The cells were centrifuged at 800 rpm for 3:30 min to collect pallets of viable cells. The collected cell palette was washed and resuspended in DMEM medium. Cells were then counted using a hemacytometer, and cell viability was analyzed through an MTT assay. The cell suspension was stored on ice until they were immediately implanted into rats. 0.1 mL of HeLa cells mixed with Matrigel were injected subcutaneously into the right and left flanks of immunocompromised rats with the following 4-day tumor implantation plan Day 1: 1×10^5 cells/3 mL (3.33×10^4/dose $\times$ 3); Day 2: 1×10^6 cells/3 mL (3.33×10^5/dose $\times$ 3); Day 3: 1×10^7 cells/3 mL (3.33×10^6/dose $\times$ 3) and Day 4: 5×10^7 cells/3 mL (1.66×10^7/dose $\times$ 3) (Cilwyn-Shalitha and Sasidharan 2023).

Investigations of tumor growth in xenograft model

Tumor growth at the site of implantation was examined with careful monitoring of clinical signs, including changes in the body weight of animals. A digital calliper was used to measure the tumor volume each week, and calculation was done using the formula (width^2 $\times$ length $\times$ 0.5). The greatest transverse diameter was measured as width, while the greatest longitudinal diameter was measured as length (LIU et al. 2017).

Hematological parameters

A complete WBC profiling included monocytes, basophils, eosinophils, neutrophils, and lymphocyte count and morphology analysis was carried out. Likewise, whole RBC profiling that included hematocrit, hemoglobin, RBC count, MCH, MCV, MCHC, RBC morphology, hemolysis, platelet count and morphology was performed on blood taken from the disease and treatment group. Liver function tests (alanine transaminase, alkaline phosphatase and aspartate aminotransferase) and kidney function tests (serum creatinine and blood urea nitrogen) were also performed (Dezayee et al. 2016; Pessini et al. 2020).

Biochemical parametric analysis

Serum was separated from plasma by centrifuging whole blood at 5000 rpm/min for ten minutes. From collected serum, antioxidant enzyme levels included reduced glutathione (GSH), superoxide dismutase (SOD), catalase (CAT), and malondialdehyde (MDA) levels in treatment, cancerous groups and control rats were analyzed. SOD levels were checked using formazan dye of the nitro blue tetrazolium (NBT) to determine optical density at 560 nm. In contrast, GSH levels were determined after the yellow color of DNTB [50, 50 (dithiobis 2-nitrobenzoic acid)] and sulfhydryl groups were obtained by determining absorbance at 412 nm. CAT concentration was determined using a previously published protocol, with H_2O_2 and MDA levels determined using Butylated hydroxytoluene (BHT) with absorbance measurement at 240 nm and 532 nm using a UV–visible spectrophotometer (Amar et al. 2019; Zahra et al. 2020).

Ex vivo NK cell activity assay

NK cell activity was analyzed by using a simple blood test (NK Vue® kit; ATGen). For analysis of NK cell activity, 100 µL of blood from control, disease and treatment groups

was incubated for 24 h with 30 µL of activator at 37 °C. Following incubation, the supernatant was collected and the release of IFN-γ was quantified by murine NK Vue kit (ATGen). All samples were incubated in an anti-murine IFN- antibody coated plate for 1 h at 25 °C. Each well was then washed 4 times, followed by addition and 1-h incubation of HRP-conjugated detection antibody. Again, each well was washed 4 times, then TMB substrate solution (3,3′,5,5′-tetramethylbenzidine) was added and incubated for 30 min. A stop solution was added, and absorbance was measured at 450 nm using an ELISA reader (Lee et al. 2021).

Histopathological analysis

At the end of the experiments, tissues from tumor sites and other vital organs were saved in 10% neutral buffer formalin. 5 µm sliced sections of tissue samples stained with hematoxylin and eosin were observed under an optical microscope (IX 51; Olympus, Tokyo, Japan) equipped with a digital camera (TL4). Micrographs were saved to confirm malignant transformation in tissues and to evaluate the therapeutic outcomes of pure NDV and HA-TC-NDV (Keshavarz et al. 2020).

Immunohistochemical assay

For antigen retrieval, the slides were processed using an enzymatic method following deparaffinization and PBS washing for 5 min, 3 times consecutively. Slides were immersed in H_2O_2 (3%) to halt any endogenous peroxidases, followed by a PBS wash. Slides were incubated with 5% normal goat serum as a blocking serum for 2 h. Afterwards, the slides were exposed to primary antibodies TNF-α, NFκB and COX-II and incubated overnight. The following day, slides were washed with PBS prior to a 90 min incubation with secondary antibody, followed by a 60 min incubation with an ABC kit (Santa Cruz) in a humidified box. Slides were washed again with PBS, stained with DAB and dehydrated by using 70, 80, 90 and 100% ethanol. After dehydration, slides were fixed with xylene, and coverslips were placed with mounting media. An inverted microscope was used to capture images in TIFF format for later analysis by ImageJ software (Ni et al. 2021).

ELISA analysis

The collected tissue samples were immediately placed on ice-cold PBS with a mixed protease inhibitor. For further homogenization, samples were kept at − 80 °C. Following this, tissue samples were placed on a shaker for 2 h and centrifuged at 4 °C at 13,000 rpm for 2 h. The supernatant was collected in prechilled tubes. ELISA was performed to analyze the expression of proteins in the systemic circulation of animal models by using a rat Calbiotech ELISA kit for BCL-2, Bax, cleaved Caspase-3 and cleaved PARP in control, diseased and treatment groups. NFκB, TNF-α and COX-II expression was also determined using a rat specific antibodies Calbiotech ELISA kit (Yang et al. 2022).

Viral RNA quantification

Using RNAeasy Mini Kit (Qiagen, USA), total RNA was extracted from tumors and organs. The RNA was used for cDNA preparation using the iScript cDNA Kit (Bio-rad, U.S.A.) following the manufacturer's protocol. The synthesized cDNA was then

subjected to PCR assay (Taqman) using (FAM)-AAGCGTTTCTGTCTCCTTCCTCCA -(BHQ)3′(probe-5′), 5′ TCCGCAAGATCCAAGGGTCT 3′ forward primer and 5′ CGCTGTTGCAACCCCAAG 3′ reverse primer. The PCR program was set at 95 °C for 4 min, followed by 40 cycles of 95 °C for 12 s, 56 °C for 32 s and 72 °C for 22 s (Mohamed Amin et al. 2019).

Statistical studies

All data collected were documented as mean ± SD. One-way ANOVA followed post hoc Bonferroni correction was implemented to evaluate the significance of differences among experimental groups. The $p \leq 0.05$ probability values were considered significant.

Acknowledgements
The authors gratefully acknowledge technical and financial support provided by Deanship of Scientific Research (DSR) at King Abdulaziz University, Jeddah, Saudi Arabia.

Author contributions
KK conducted major study including designing and execution of experiments. FN provided support in in silico analysis, nanoparticle preparation and characterization. MSA contributed in data analysis, investigation, methodology and funding, TA and SA proofread this article and supervised this project.

Funding
The Deanship of Scientific Research (DSR) at King Abdulaziz University, Jeddah, Saudi Arabia, has funded this project, under grant no. (FP-249-43).

Availability of data and materials
All data generated or analyzed during this study are included in this published article.

Declarations

Ethics approval and consent to participate
Not applicable.

Consent for publication
Not applicable.

Competing interests
The authors declare that they have no competing interests.

Received: 5 June 2023 Accepted: 8 July 2023
Published online: 12 August 2023

References

Aghasizadeh M, Moghaddam T, Bahrami A, Sadeghian H, Alavi S, Matin M (2022) 8-Geranyloxycarbostyril as a potent 15-LOX-1 inhibitor showed great antitumor effects against prostate cancer. Life Sci 293:120272
Amar S, Eryilmaz R, Demir H, Aykan S, Demir C (2019) Determination of oxidative stress levels and some antioxidant enzyme activities in prostate cancer. Aging Male 22(3):198–206
Baranov MV, Kumar M, Sacanna S, Thutupalli S, van den Bogaart G (2021) Modulation of immune responses by particle size and shape. Front Immunol 11:607945
Burman B, Pesci G, Zamarin D (2020) Newcastle disease virus at the forefront of cancer immunotherapy. Cancers 12(12):3552. https://doi.org/10.3390/cancers12123552
Burton C, Bartee E (2019) Syncytia formation in oncolytic virotherapy. Mol Ther Oncolytics 15:131–139. https://doi.org/10.1016/j.omto.2019.09.006
Cao H-Z, Zheng P-S, Yang W-T (2021) Cytotoxic effect of disulfiram/copper on human cervical cancer cell lines and LGR5-positive cancer stem-like cells. BMC Cancer. https://doi.org/10.21203/rs.3.rs-1122434/v1
Chan L-C, Kalyanasundram J, Leong S-W, Masarudin MJ, Veerakumarasivam A, Yusoff K, Chan S-C, Chia S-L (2021) Persistent Newcastle disease virus infection in bladder cancer cells is associated with putative pro-survival and anti-viral transcriptomic changes. BMC Cancer 21(1):625. https://doi.org/10.1186/s12885-021-08345-y
Chen Y, Zhu S, Pei Y, Hu J, Hu Z, Liu X, Wang X, Gu M, Hu S, Liu X (2021) Differential microrna expression in Newcastle disease virus-infected HeLa cells and its role in regulating virus replication. Front Oncol 11:616809. https://doi.org/10.3389/fonc.2021.616809
Cilwyn-Shalitha B, Sasidharan S (2023) Mechanisms of the *in vivo* antitumor activity of *Polyalthia longifolia* leaf extract against HeLa cell xenograft tumor: a microscopic-based histological and immunohistochemical Microanalyses. Microsc Microanal. https://doi.org/10.1093/micmic/ozad023

Dezayee ZMI, Al-Nimer MSM (2016) The clinical importance of measurement of hematological indices in the breast cancer survivals: a comparison between premenopausal and postmenopausal women. World J Oncol 7(1):1–4. https://doi.org/10.14740/wjon956e
Diehl R, Ferrara F, Müller C et al (2017) Immunosuppression for in vivo research: state-of-the-art protocols and experimental approaches. Cell Mol Immunol 14:146–179. https://doi.org/10.1038/cmi.2016.39
Fulber JPC, Farnós O, Kiesslich S, Yang Z, Dash S, Susta L, Wootton SK, Kamen AA (2021) Process development for Newcastle disease virus-vectored vaccines in serum-free vero cell suspension cultures. Vaccines 9(11):1335. https://doi.org/10.3390/vaccines9111335
Global Cancer Observatory. 2020. Global Cancer Observatory. Iarc.fr. 2020. https://gco.iarc.fr/.
Gu Y, Wen H, Zhang Y, Bai L, Zhou Y, Zhang H, Tian L, Hao J, Liu Y (2021) Studies of anticancer activity in vivo and in vitro behaviors of liposomes encapsulated iridium(iii) complex. J Biol Inorg Chem 26(1):109–122. https://doi.org/10.1007/s00775-020-01841-9
Hasanifard M, Ebrahimi-Hosseinzadeh B, Hatamian-Zarmi A, Rezayan AH, Esmaeili MA (2017) Development of thiolated chitosan nanoparticles based mucoadhesive vaginal drug delivery systems. Polym Sci Ser A 59(6):858–865
Hu J, Wang H, Gu J, Liu X, Zhou X (2018) Trail armed oncolytic Poxvirus suppresses lung cancer cell by inducing apoptosis. Acta Biochim Biophys Sin 50(10):1018–1027. https://doi.org/10.1093/abbs/gmy096
"Human Papillomavirus and Related Diseases Report ASIA." n.d. Accessed 28 Dec 2019. https://hpvcentre.net/statistics/reports/XSX.pdf.
Keshavarz M, Nejad ASM, Esghaei M, Bokharaei-Salim F, Dianat-Moghadam H, Keyvani H, Ghaemi A (2020) Oncolytic Newcastle disease virus reduces growth of cervical cancer cell by inducing apoptosis. Saudi J Biol Sci 27(1):47–52. https://doi.org/10.1016/j.sjbs.2019.04.015
Kousar K, Naseer F, Abduh MS, Kakar S, Gul R, Anjum S, Ahmad T (2023) Green synthesis of hyaluronic acid coated, thiolated chitosan nanoparticles for CD44 targeted delivery and sustained release of Cisplatin in cervical carcinoma. Front Pharmacol 13:1073004. https://doi.org/10.3389/fphar.2022.1073004
Lee Y, Shin H, Kim J (2021) In vivo anticancer effects of resveratrol mediated by NK. Cell Activation J Innate Immun 13(2):94–106. https://doi.org/10.1159/000510315
Lei C, Yang J, Hu J, Sun X (2021) On the calculation of TCID50 for quantitation of virus infectivity. Virol Sin 36(1):141–144. https://doi.org/10.1007/s12250-020-00230-5
Liddicoat AM, Lavelle EC (2019) Modulation of innate immunity by cyclosporine a. Biochem Pharmacol 163:472–480. https://doi.org/10.1016/j.bcp.2019.03.022
Liu A, Zheng R, Yang F, Huang L, Zhang L, Zhang J (2017) Effects of curcumin on growth of human cervical cancer xenograft in nude mice and underlying mechanism. Food Sci Technol 38(1):106–111. https://doi.org/10.1590/1678-457x.02817
Liu T, Zhang Y, Cao Y, Jiang S, Sun R, Yin J, Gao Z, Ren G, Wang Z, Yu Q, Sui G, Sun X, Sun W, Xiao W, Li D (2020) Optimization of oncolytic effect of Newcastle Disease Virus Clone30 by selecting sensitive tumor host and constructing more oncolytic viruses. Gene Ther 28(12):697–717. https://doi.org/10.1038/s41434-020-0145-9
Loutfy SA, Abdel-Salam AI, Moatasim Y, Gomaa MR, Abdel Fattah NF, Emam MH, Ali F, ElShehaby HA, Ragab EA, Alam El-Din HM, Mostafa A, Ali MA, Kasry A (2022) Antiviral activity of chitosan nanoparticles encapsulating silymarin (Sil-CNPs) against SARS-CoV-2 (in silico and in vitro study). RSC Adv 12(25):15775–15786. https://doi.org/10.1039/d2ra00905f
Madar I, Sultan G, Chelliah R, Oh DH (2022) Screening for anticancer activity: trypan blue exclusion assay. In: Dharumadurai D (ed) Methods in actinobacteriology. Springer, New York. https://doi.org/10.1007/978-1-0716-1728-1_59
Mesas C, Martínez R, Doello K, Ortiz R, López-Jurado M, Bermúdez F, Quiñonero F, Prados J, Porres JM, Melguizo C (2022) In vivo antitumor activity of Euphorbia lathyris ethanol extract in colon cancer models. Biomed Pharmacother 149:112883. https://doi.org/10.1016/j.biopha.2022.112883
Mohamed Amin Z, Che Ani MA, Tan SW, Yeap SK, Alitheen NB, Syed Najmuddin SU, Kalyanasundram J, Chan SC, Veerakumarasivam A, Chia SL, Yusoff K (2019) Evaluation of a recombinant Newcastle disease virus expressing human IL12 against human breast cancer. Sci Reports 9(1):13999. https://doi.org/10.1038/s41598-019-50222-z
Morla S, Kumar A, Kumar S (2019) Newcastle disease virus mediated apoptosis and migration inhibition of human oral cancer cells: a probable role of β-catenin and matrix metalloproteinase-7. Sci Rep 9(1):10882. https://doi.org/10.1038/s41598-019-47244-y
Naseer F, Ahmad T, Kousar K, Kakar S, Gul R, Anjum S, Shareef U (2023) Formulation for the targeted delivery of a vaccine strain of oncolytic measles virus (OMV) in hyaluronic acid coated thiolated chitosan as a green nanoformulation for the treatment of prostate cancer: a viro-immunotherapeutic approach. Int J Nanomed 18:185–205. https://doi.org/10.2147/ijn.s386560
Ni J, Feng H, Xu X, Liu T, Ye T, Chen K, Li G (2021) Oncolytic vaccinia virus harboring *Aphrocallistes vastus* lectin inhibits the growth of cervical cancer cells HeLa S3. Mar Drugs 19(10):532. https://doi.org/10.3390/md19100532
Pessini PGDS, Knox de Souza PR, Chagas CDS, Sampaio EG, Neves DS, Petri G, Fonseca FLA, da Silva EB (2020) Hematological reference values and animal welfare parameters of BALB/C-FMABC (*Mus musculus*) inoculated with Ehrlich tumor kept in the vivarium at ABC Medical School. Anim Models Exp Med 3(1):32–39. https://doi.org/10.1002/ame2.12099
Puluhulawa LE, Joni IM, Elamin KM, Mohammed AF, Muchtaridi M, Wathoni N (2022) Chitosan–hyaluronic acid nanoparticles for active targeting in cancer therapy. Polymers 14(16):3410. https://doi.org/10.3390/polym14163410
Ramakrishnan MA (2016) Determination of 50% endpoint titer using a simple formula. World J Virol 5(2):85–86. https://doi.org/10.5501/wjv.v5.i2.85
Sayyed AA, Gondaliya P, Mali M, Pawar A, Bhat P, Khairnar A, Arya N, Kalia K (2021) Mir-155 inhibitor-laden exosomes reverse resistance to Cisplatin in a 3D tumor spheroid and xenograft model of oral cancer. Mol Pharm 18(8):3010–3025. https://doi.org/10.1021/acs.molpharmaceut.1c00213.s001
Schirrmacher V, Fournier P (2009) Newcastle disease virus: a promising vector for viral therapy, immune therapy, and gene therapy of cancer. Gene therapy of cancer. Humana Press, Iotowa, pp 565–605. https://doi.org/10.1007/978-1-59745-561-9_30

Schmidt MW, Battista MJ, Schmidt M, Garcia M, Siepmann T, Hasenburg A, Anic K (2022) Efficacy and safety of immunotherapy for cervical cancer—a systematic review of clinical trials. Cancers 14(2):441. https://doi.org/10.3390/cancers14020441

Seyed-Khorrami S-M, Soleimanjahi H, Soudi S, Habibian A (2021) MSCs loaded with oncolytic reovirus: Migration and in vivo virus delivery potential for evaluating anti-cancer effect in tumor-bearing C57BL/6 mice. Cancer Cell Int 21(1):244. https://doi.org/10.1186/s12935-021-01848-5

Shin DH, Nguyen T, Ozpolat B, Lang F, Alonso M, Gomez-Manzano C, Fueyo J (2021) Current strategies to circumvent the antiviral immunity to optimize cancer virotherapy. J ImmunoTher Cancer 9(4):e002086. https://doi.org/10.1136/jitc-2020-002086

Vijayakumar G, Zamarin D (2019) Design and production of Newcastle Disease Virus for intratumoral immunomodulation. Methods Mol Biol 2058:133–154. https://doi.org/10.1007/978-1-4939-9794-7_9

Yan H, Lu J, Wang J, Chen L, Wang Y, Li L, Miao L, Zhang H (2021) Prevention of cyclophosphamide-induced immunosuppression in mice with traditional Chinese medicine Xuanfei Baidu decoction. Front Pharmacol 12:730567. https://doi.org/10.3389/fphar.2021.730567

Yang CM, Yang CC, Hsu WH, Hsiao LD, Tseng HC, Shih YF (2022) Tumor necrosis factor-α-induced C–C motif chemokine ligand 20 expression through TNF receptor 1-dependent activation of EGFR/p38 MAPK and JNK1/2/FoxO1 or the NF-κB pathway in human cardiac fibroblasts. Int J Mol Sci 23(16):9086. https://doi.org/10.3390/ijms23169086

Yoon J, Kim H, Jeong YI, Yang HS (2022) CD44 receptor-mediated/reactive oxygen species-sensitive delivery of nanophotosensitizers against cervical cancer cells. Int J Mol Sci 23(7):3594. https://doi.org/10.3390/ijms23073594

Zahra K, Patel S, Dey T, Pandey U, Mishra SP (2020) A study of oxidative stress in cervical cancer- an institutional study. Biochem Biophy Reports 25:100881. https://doi.org/10.1016/j.bbrep.2020.100881

Zani AP, Zani CP, Din ZU, Rodrigues-Filho E, Ueda-Nakamura T, Garcia FP, de Oliveira Silva S, Nakamura CV (2023) Dibenzylideneacetone induces apoptosis in cervical cancer cells through ros-mediated mitochondrial damage. Antioxidants 12:317. https://doi.org/10.3390/antiox12020317

Publisher's Note